High-Order Compact Difference Methods for Glow Discharge Modeling

Jonathan Poggie*
Air Force Research Laboratory, Wright-Patterson AFB, Ohio 45433-7512 USA

This paper explores the feasibility of applying high-order, compact difference methods to the modeling of glow discharges for high-speed flow control. Previous papers (AIAA 2007-0632, 2008-1357) have successfully applied second-order finite difference methods to glow discharge modeling. Detailed grid resolution studies, however, have revealed that very fine grid resolution is required for acceptable quantitative results. High-order compact difference methods offer a possible means of achieving high spatial accuracy on coarser grids, potentially leading to a significant reduction in the computational cost of an accurate solution. Sample compact difference calculations are presented here for one-dimensional test cases, and accuracy is compared to a standard second-order upwind scheme. In particular, fourth order accuracy is demonstrated with compact differencing for several problems involving the internal structure of weak shocks and the plasma-sheath transition. Future work will focus on applying the compact difference method to problems of interest in plasma aerodynamics.

I. Introduction

Since the mid-1990s, there has been considerable research interest in plasma-based flow control techniques for aerospace applications. Because of their favorable weight and power consumption properties, small-scale actuators based on glow and arc discharges have become increasingly popular, and much effort has been put toward numerical modeling of actuator behavior.[1–3]

Toward this end, the author has developed a second-order accurate, finite-difference code capable of modeling the region of finite space-charge present in the vicinity of electrode surfaces in the electric discharges used for flow control.[3–5] The physical model includes the fluid conservation laws for the bulk gas flow, a model for charged particle motion, and a self-consistent computation of the electric potential. This code has been successfully applied to a variety of discharge problems, including low-density plasma-sheath problems, DC glow discharges, and RF glow discharges. Comparisons among different numerical methods have been carried out, and a central difference scheme, an upwind scheme, and a finite difference implementation of the Sharfetter-Gummel scheme have all been found to give very similar results.

Recently, an investigation was carried out on spatial resolution issues in modeling DC glow discharges.[4,5] A detailed grid resolution study was carried out, and very fine grid resolution was found to be required for acceptable quantitative results. Coarse grids led to underestimates of number density, temperature, and current density and to overestimates of the lateral extent of the discharge column.

High-order compact difference methods[6,7] offer a possible means of achieving high spatial accuracy on coarser grids, potentially leading to a significant reduction in computational cost. This paper presents a preliminary, one-dimensional implementation of a compact difference scheme for plasma discharge problems. Sample calculations are presented here for several test problems, including shock internal structure and the plasma-sheath transition.

II. Methods

The physical model and the numerical methods are described in this section. The physical model includes the fluid conservation laws for the motion of each species and a self-consistent computation of the electric potential. The numerical implementation involves compact spatial differences of up to sixth order accuracy, driven by a low-storage, fourth-order Runge-Kutta time marching scheme.

*Senior Aerospace Engineer, Computational Sciences Branch, AFRL/RBAC, 2210 Eighth St., Associate Fellow AIAA.
Cleared for public release, distribution unlimited (88ABW-2008-1309).

A. Physical Model

Continuum methods, based on moments of the Boltzmann equation, have been a popular and productive means of modeling electrical discharges. One-dimensional modeling of direct-current glow discharges was carried out as early as the late 1950s,[8,9] and two-dimensional simulations were first carried out in the late 1980s.[10,11] By the early 1990s, two dimensional simulations of radio-frequency glow discharges[12,13] and transient low-density discharges[14,15] were done. Three-dimensional simulations have appeared more recently.[3,16]

A variety of physical models have been employed in such work. One of the most common models is drift-diffusion, assuming local equilibrium with the electric field, so all coefficients are a function of the local reduced field E/N.[9–11] The next step up in generality is to solve the electron energy equation as well, and use the local electron temperature T_e instead of the local E/N to determine the transport and ionization coefficients.[17,18]

Some studies have used continuity-momentum equations in place of the drift-diffusion model, thus including the effects of particle momentum. The role of inertia in DC and RF discharges has been examined, including the momentum of the electrons,[19] the heavy particles,[20] or both.[21,22] Ion inertia is important in the transient sheath that appears in plasma-source ion implantation,[23] and in modeling the low-density plasma-sheath transition.[24,25]

One aim of this ongoing project is to determine limits of the moment method in modeling electrical discharges, specifically whether a three-moment model for each species can be accurate and computationally tractable. A relatively general formulation of the conservation equations for electrical discharges is outlined below, based on standard references.[26–28] Briefly, the conservation laws can be derived from moments of the Boltzmann equation, with closure models utilized for the inelastic collision source terms,[26] the elastic collision source terms,[26,29] and the flux terms.[27,30,31] In this preliminary work, a one-dimensional form of these equations is used, suitable for the test problems of shock internal structure and the plasma-sheath transition investigated in this paper.

1. Governing Equations

The focus of this paper is on one-dimensional shock and sheath structure in ionized argon. Gravity is neglected, and the absence of an applied magnetic field is assumed. The conservation equations for each species are:

$$\begin{aligned}
\frac{\partial}{\partial t}(m_s n_s) + \frac{\partial}{\partial x}(m_s n_s u_s) &= S_s \\
\frac{\partial}{\partial t}(m_s n_s u_s) + \frac{\partial}{\partial x}(m_s n_s u_s^2 + n_s k_B T_s) &= \frac{\partial}{\partial x}\left[\tfrac{4}{3}\mu_{vs}\frac{\partial u_s}{\partial x}\right] + q_s n_s E + A_s \\
\frac{\partial}{\partial t}\left[n_s\left(H_s + \frac{k_B T_s}{\gamma_s - 1} + \tfrac{1}{2}m_s u_s^2\right)\right] + \frac{\partial}{\partial x}\left[n_s u_s\left(H_s + \frac{\gamma_s k_B T_s}{\gamma_s - 1} + \tfrac{1}{2}m_s u_s^2\right)\right] &= \\
\frac{\partial}{\partial x}\left[\tfrac{4}{3}\mu_{vs}u_s\frac{\partial u_s}{\partial x} + k_s\frac{\partial T_s}{\partial x}\right] + q_s n_s u_s E + M_s &
\end{aligned} \tag{1}$$

where the notation $s = n, i, e$ indicates the neutrals, ions, and electrons, respectively.

The mass per particle of each species is denoted as m_s, and the corresponding charge per particle is $q_n = 0$, $q_i = +e$, and $q_e = -e$. The number density is n_s, the velocity is u_s, and the translational temperature is T_s. The viscosity and thermal conductivity of each species are denoted as μ_{vs} and k_s, respectively. The electric field is E, and the symbol k_B indicates the Boltzmann constant. The internal energy per particle is assumed to have the form $m_s\epsilon_s = H_s + k_B T_s/(\gamma_s - 1)$, where $\gamma_s = 5/3$ is the ratio of specific heats. The heat of formation is $H_n = H_e = 0$ and $H_i = \mathcal{H}$, where $\mathcal{H} = 15.7$ eV for argon ionization.

It assumed that the gas is weakly ionized, so that the primary elastic collisions are with neutral particles. For the inelastic collisions, it is assumed that the species appear or disappear with the average momentum and energy of their peers, except for the electrons, which lose energy $\mathcal{H}$ in each inelastic collision.

Consider the reaction pair $\mathrm{Ar} + \mathrm{e}^- \rightleftharpoons \mathrm{Ar}^+ + 2\mathrm{e}^-$ and let ω be the production rate of charged particles. The species source terms become:

$$\begin{aligned}
S_i &= m_i\omega \\
S_e &= m_e\omega \\
S_n &= -m_n\omega
\end{aligned} \tag{2}$$

The momentum source terms are:

$$\begin{aligned}
A_i &= \omega m_i u_i - n_i m_{in}\nu_{in}(u_i - u_n) \\
A_e &= \omega m_e u_e - n_e m_{en}\nu_{en}(u_e - u_n) \\
A_n &= -(A_i + A_e)
\end{aligned} \tag{3}$$

The energy source terms are:

$$\begin{aligned} M_i &= \omega\left(\mathcal{H} + \frac{k_B T_i}{\gamma_i - 1} + \tfrac{1}{2} m_i u_i^2\right) - \frac{n_i m_{in} \nu_{in}}{m_i + m_n}\left[3k_B(T_i - T_n) + (u_i - u_n)(m_i u_i + m_n u_n)\right] \\ M_e &= -\omega\mathcal{H} + \omega\left(\frac{k_B T_e}{\gamma_e - 1} + \tfrac{1}{2} m_e u_e^2\right) - \frac{n_e m_{en} \nu_{en}}{m_e + m_n}\left[3k_B(T_e - T_n) + (u_e - u_n)(m_e u_e + m_n u_n)\right] \\ M_n &= -(M_i + M_e) \end{aligned} \tag{4}$$

To complete the physical model, the electric field must be found from a consistent solution of Maxwell's equations. For the present work, the Poisson equation is solved for the electric potential:

$$\frac{\partial^2 \phi}{\partial x^2} = -\frac{1}{\epsilon_0} \sum_s q_s n_s \tag{5}$$

and the electric field is found from $E = -\partial\phi/\partial x$.

Some calculations were carried out with the full model (1)-(5), but for the work presented in this paper, Boltzmann equilibrium was assumed for the electrons in order to reduce the computational cost of carrying out many runs for convergence studies. Under this the assumption, the electron temperature is held fixed, and the electron number density is computed from:

$$n_e = n_o \exp\left(\frac{e\phi}{k_B T_e}\right) \tag{6}$$

where n_0 is a reference number density, corresponding to the potential $\phi = 0$.

2. Transport Properties and Reaction Rates

The collision frequency between the charged and neutral species ν_{sn} was estimated from mobility data, with the correlations for ion and electron mobility in argon taken from Ward.[8]

For the ionization rates, two models were considered. One had the form $\omega = z n_e$, where the ionization rate z is an eigenvalue of the problem, the production rate necessary to maintain a steady state. Alternatively, ionization and recombination coefficients were taken from the correlations of Adamovich et al.[32]

Standard correlations were used for the viscosity and thermal conductivity of the neutral particles.[33] The viscosity and thermal conductivity of the charged particles were neglected for the present work. A reasonable estimate of their magnitudes[21,30] can be found by assuming that the ions have the same transport coefficients as the neutrals, and that the electron transport coefficients can be found by assuming a Lewis number of unity and a Prandtl number of $2/3$.

3. Nondimensionalization

The equations were solved in non-dimensional form. For brevity, only an outline of the nondimensionalization procedure is given here. Global reference quantities were chosen for length L_R, velocity u_R, number density n_R, potential ϕ_R, collision rate ν_R, viscosity μ_{vR}, and thermal conductivity k_R. For each species, however, there was a different reference density $\rho_{Rs} = m_s n_R$, temperature $T_{Rs} = m_s u_R^2/k_B$, and pressure $p_{Rs} = m_s n_R u_R^2$. Space charge was normalized by the electron charge e, and heat of formation was normalized by $m_s u_R^2$.

The nondimensionalized equations have much the same form as (1)-(5). In addition to a Reynolds number and Prandtl number for each species, the following nondimensional parameters appeared as a consequence of this form of nondimensionalization:

$$\Phi_s = \frac{e\phi_R}{m_s u_R^2} \quad C = \frac{\nu_R L_R}{u_R} \quad a = L_R\sqrt{\frac{e n_R}{\epsilon_0 \phi_R}}$$

The nondimensional parameters are, respectively, a relative field strength, a nondimensional collision frequency parameter, and a non-neutrality parameter.

B. Numerical Methods

The governing equations (1)-(4) were solved using a fourth-order accurate, low-storage Runge-Kutta time marching scheme combined with either a second-order Steger-Warming scheme or a compact spatial scheme of up to sixth order accuracy. For the compact scheme, stability was enforced by filtering, typically with a filter of two orders greater than the accuracy of the basic scheme. The Poisson equation (5) was solved by an iterative scheme (described below),

with either second-order central or compact spatial differences. The Poisson solution was not filtered. For the present examples, a one-dimensional, uniform mesh was employed, but an extension of the method to multi-dimensional, curvilinear grids is planned for future work.

1. Governing Equations

The conservation laws (1) can be written in the form:

$$\frac{\partial U}{\partial t} + \frac{\partial E}{\partial x} = \frac{\partial E_v}{\partial x} + S \tag{7}$$

where U is the vector of conserved variables, E is the inviscid flux vector, E_v is the viscous flux vector, and S represents the source terms. A standard, low-storage, fourth-order Runge-Kutta scheme[34] was used for time integration of Eq. (7). Two different schemes were used to evaluate the spatial differences: either a compact difference scheme of up to sixth-order accuracy (described below), or a second-order Steger-Warming scheme, which used third-order MUSCL extrapolation[35] for the inviscid fluxes and second-order central differencing for the viscous terms.

The Poisson equation (5) was solved at the end of each stage of the Runge-Kutta time-integration. It can be written in the form:

$$\frac{\partial^2 \phi}{\partial x^2} = S_\phi \tag{8}$$

An iteration procedure was introduced such that the potential at step m was $\phi^{m+1} = \phi^m + \Delta\phi$. With a linear expansion about the solution from the previous iteration, the discretized equation has the form:

$$\left[1 - \Delta\tau\delta_x^2 + \Delta\tau\frac{\partial S_\phi}{\partial \phi}\right]\Delta\phi = \omega\Delta\tau\left[\delta_x^2\phi^m - S_\phi^m\right] \tag{9}$$

with iteration driving $\Delta\phi$ to zero. Here τ is a time-like variable introduced to motivate the iteration process, and ω is an over-relaxation factor. Discretizing the left-hand side using second order central differences in space, a tridiagonal system of equations is obtained. (Since iteration drives $\Delta\phi$ to zero, the form of the discretization of the left-hand-side does not affect the order of spatial accuracy of the converged solution.) Either central or compact difference schemes were used to evaluate the spatial differences present on the right hand side of Eq. (9), and the system was solved using the Thomas tridiagonal algorithm.[36] Iteration was continued until the change in potential $\Delta\phi$ was less than a small tolerance.

2. Compact Differences

Considering a one-dimensional, uniform mesh, the following central difference scheme[6,7] with a 5-point stencil can be used to generate estimates of the first derivative $\phi' = \partial\phi/\partial x|_i$ with up to sixth-order accuracy:

$$\alpha\phi'_{i-1} + \phi'_i + \alpha\phi'_{i+1} = a\frac{\phi_{i+1} - \phi_{i-1}}{2\,\Delta x} + b\frac{\phi_{i+2} - \phi_{i-2}}{4\,\Delta x} \tag{10}$$

Here α, a, and b are constants that are used to alter the properties of the scheme, and $\phi(x)$ is a generic function, not to be confused with the electric potential. Taylor series expansions can be used to derive a family of second to sixth order accurate schemes employing this template.[6,7] Table 1 gives selected coefficients for internal points using Eq. (10) for different orders of accuracy. Note that the implicit form of the scheme ($\alpha \neq 0$) results in a narrower stencil for a given order of accuracy that for an explicit form ($\alpha = 0$). Modified schemes[7] were used near boundaries, where the interior stencil would protrude outside of the domain.

Table 2 shows the forms of the compact difference scheme that were examined in this project, using the notation of Gaitonde and Visbal. To evaluate the derivative at each point, the appropriate form of Eq. (10) was solved using the Thomas tridiagonal algorithm.[36] Second derivatives were evaluated by applying the differencing scheme twice.

Figure 1 illustrates the accuracy of each of the schemes (see Table 2) in computing the derivative of the function $f(x) = \sin x$ in the range $0 \leq x \leq \pi$. The L_2-norm for the full domain is shown in Fig. 1a. With this metric of solution quality, the accuracy is seen to be constrained by the lower order stencil used near the boundaries. If points near the boundary are omitted from the norm (Fig. 1b), the convergence rate is seen to improve, and the accuracy of the scheme E4-AC4-C6-AC4-E4 is seen to lie between that of pure fourth- and sixth-order schemes.

Numerical stability was enforced using filtering, typically with a filter of two orders greater than the accuracy of the basic scheme. The form of the filtering scheme[7] for interior points was as follows:

$$\alpha_f \overline{\phi}_{i-1} + \overline{\phi}_i + \alpha_f \overline{\phi}_{i+1} = \sum_{n=0}^{N} \frac{a_n}{2} (\phi_{i+n} + \phi_{i-n}) \tag{11}$$

where $\overline{\phi}_i$ is the filtered value of ϕ_i, and $N+1$ is the order of the filter. A table of coefficients for interior-point filters of second to eighth order is given in Table 3. Modified filters were used near the boundaries; the various options are shown in Table 2. (In the table, F0 indicates that no filter was applied to the boundary points.) The filter was applied to each primitive variable at the end of a time step, and the boundary conditions were updated so that the boundary points were consistent with the filtered interior points. For the cases labeled Filter A in Table 2, the filter's free parameter was set to $\alpha = 0.40$, whereas for Filter B, the value was varied between $\alpha = 0.49$ at the boundary and $\alpha = 0.40$ for the interior points.

Careful treatment of the boundary conditions was necessary to maintain the spatial accuracy of the scheme. Unless otherwise noted, both extrapolation and derivative (Neumann) boundary conditions were handled with a scheme of spatial order corresponding to that of the boundary scheme.

III. Results

Several test problems were examined in order to evaluate the accuracy of the compact scheme relative to the second-order Steger-Warming scheme. The focus was on one-dimensional shock and sheath structure in ionized argon.

A. Neutral-Gas Shock

As a test of the code's ability to solve electrically-neutral, viscous gasdynamics problems, a calculation was carried out of the internal structure of a weak shock in argon. The following notation will be used: the subscript 1 indicates the state upstream of the shock, 2 indicates the downstream state, m indicates an average of the upstream and downstream states, and $x_{1/2}$ indicates the position corresponding to $u = u_m$. The upstream Mach number was $M_1 = 1.2$. The dimensional upstream conditions were: $p_1 = 42.2$ kPa, $T_1 = 125$ K, $u_1 = 125$ m/s. Downstream conditions were computed using the ideal gas jump conditions.[37] The computational domain was $L = 5$ μm in width.

A reference computation was carried out with 401 points using the E4-AC4-C6-AC4-E4 compact difference scheme. Figure 2a shows the basic shock structure, with the independent variables normalized using the conditions upstream of the shock. Pressure, temperature, and density increase monotonically through the shock, whereas velocity decreases to satisfy continuity. Because of the effects of heat conduction, entropy has the characteristic maximum typical of shock structure (See Zel'dovich and Raizer,[38] pp. 473–475). The total enthalpy, $H = e + p/\rho + u^2/2$, has a slight variation through the shock, and the upstream and downstream values are equal: $H_1 = H_2$.

As a qualitative verification of code accuracy, the reference solution is compared to the approximate analytical solution of G. I. Taylor in Fig. 2b. (See Thompson,[39] pp. 361-368, for a full discussion of the Taylor weak shock theory. In the figure, $A = (\gamma+1)/[8/3 + 2(\gamma-1)/\mathrm{Pr}] \approx 4/7$.) Although the analytical solution cannot be used for a quantitative verification of the code because of its approximate nature, the agreement between the numerical and analytical solutions is seen to be quite good. In particular, the shock thickness is predicted accurately.

The shock thickness based on the total enthalpy profile was chosen as a parameter for studying the convergence of the scheme. This thickness was defined as: $\Delta_H = \int_{-\infty}^{\infty} (H - H_1)/H_1 \; dx$. Since the total enthalpy upstream and downstream of the shock are equal in the present problem, the integrand is zero at the boundaries of the domain. Integration was carried out using Eq. (13), below. Grid convergence was studied using this parameter for two numerical schemes: the E4-AC4-C6-AC4-E4 compact difference scheme and the second-order accurate Steger-Warming scheme. Figure 2c shows the percentage error in the total enthalpy thickness, with the reference solution used as the baseline. The remarkable accuracy of the compact scheme relative to the Steger-Warming scheme is apparent in the plot. Note the difference in accuracy between the two filters used with the compact scheme.

B. Transient Sheath Problem

As a test of the coupled potential and moment equations, this section investigates the effect of a suddenly-applied voltage on an initially-uniform, low-density plasma. This transient sheath problem was used as a test case in previous papers.[40,41]

A two-moment model was considered for the this problem. The ion and electron temperatures were held fixed at $T_i = 293$ K and $T_e = 11600$ K, respectively, and the electron number density was computed by assuming Boltzmann equilibrium, Eq. (6). Viscous forces and collisions with neutrals were neglected for the ions. This restricted model was implemented in the code by turning off selected terms in the full model.

The initial condition was taken to be a stationary, uniform plasma of number density $n_0 = 1 \times 10^{14}$ m^{-3}, and a potential of $\phi = -50$ V was suddenly applied at the left electrode ($x = 0$) at time $t = 0$. The potential at the right boundary of the computational domain was held fixed at zero.

The characteristic scales in this problem are the ion plasma frequency $f_p = \sqrt{n_o e^2/(4\pi^2 \epsilon_0 m_i)}$, the Bohm velocity $u_B = \sqrt{k_B T_e/m_i}$, and the electron Debye length $\lambda_D = \sqrt{\epsilon_0 k_B T_e/(n_0 e^2)}$. The computational domain was taken to be $L = 200\lambda_{De}$ wide. The ion properties at $x = 0$ were found by extrapolation (with an order of accuracy corresponding to that of the numerical scheme at the boundary), and the properties at $x = L$ of the computational domain were held fixed at $n_i = n_0$ and $u_i = 0$.

Figure 3a shows the distribution of ion and electron number densities at selected times for a reference calculation with the E4-AC4-C6-AC4-E4 compact difference scheme with a grid of 401 points and a nondimensional time step of $f_p \Delta t = 0.01$. With the sudden application of a negative potential, the electrons are repelled from the electrode, forming a layer of positive charge. The relatively massive ions slowly respond to the changed conditions, forming an ion current into the electrode. As a result, the space charge diminishes, and the sheath expands. Ahead of the sheath, a quasi-neutral presheath propagates into the bulk plasma.

The time-evolution of the ion current density $j_i = en_i|u_i|$ at the electrode is shown in Fig. 3b. The inset shows the long-time behavior on an expanded time scale. There is an initial surge in current as the transient sheath forms, followed by a gradual relaxation to constant current density at large times. In this asymptotic state, the current to the electrode is balanced by ions uncovered by the expanding rarefaction wave. The presheath accelerates the ions up to approximately the Bohm velocity, supporting a quasi-steady sheath.

The transient sheath problem was studied analytically by Lieberman,[42] who developed approximate expressions for the time-evolution of the ion current density at the cathode. Lieberman used a matrix sheath model for the short-time behavior, and a Child law sheath model for the long-time solution. Qualitative agreement between the numerical solution and Lieberman's theory is seen in Fig. 3b. (This is the level of agreement seen by Lieberman as well.)

As a gauge of the quality of the solution for different numerical schemes, the ion current at $x = 0$ and $f_p t = 24$ was examined. The error in this quantity, relative to the reference solution, is plotted versus grid size in Fig. 3c. The Steger-Warming scheme and the E4-AC4-C6-AC4-E4 compact scheme with Filter A appear to converge, respectively, with the expected second and fourth order accuracy. The compact scheme with Filter B has a high absolute accuracy, but the slope does not have the expected value.

C. Steady-State Sheath

As a somewhat more complex test case, the problem of an ionized gas confined between a pair of planar electrodes fixed at a distance of $2L$ apart was considered. The electrodes were assumed to be maintained at a constant negative potential, and to draw a current that was maintained by 'direct' ionization.

In order to exercise more features of the code, a three-moment model of ion motion was considered, along with constant temperature, Boltzmann electrons and a uniform, neutral background gas at rest. Viscous forces on the ions were neglected. The ionization rate was taken to have the form $\omega = zn_e$. As in the previous case, this restricted model was implemented in the code by turning off selected terms in the full model.

The ion properties at $x = 0$ were found by extrapolation, whereas the following conditions were imposed at the symmetry plane ($x = L$): $n_i = n_0$, $\partial u_i/\partial x = z$, and $\partial T_i/\partial x = 0$. (The boundary conditions were imposed with an order of accuracy corresponding to that of the numerical scheme at the boundary.) The centerline boundary condition on the velocity follows from applying the symmetry conditions, and has been found to be more stable than directly imposing $u_i = 0$. The boundary conditions on the electric potential were $\phi(0) = -50$ V and $\phi(L) = 0$.

The temperatures of the neutral gas and the electrons were taken to be $T_n = 293$ K and $T_e = 11600$ K, respectively. The centerline number density was $n_0 = 1 \times 10^{14}$ m^{-3}. The neutral gas pressure was taken to be $p_n = 50$ mPa.

A procedure based on the integral form of the ion continuity equation was used to estimate, at each time step, the ionization frequency z required to achieve a steady state. Assuming a steady state, and integrating the ion continuity equation (1a) from the wall at $x = 0$ to the center at $x = L$, the following formula is obtained for the ionization rate:

$$z = \frac{-n_i u_i|_{x=0}}{\int_0^L n_e \, dx} \tag{12}$$

A new value of z was computed at the end of each time step from Eq. (12). In order to make the order of accuracy of the integration in Eq. (12) consistent with compact difference schemes of up to sixth order accuracy, the following integration formula was employed:

$$\int_{x_0}^{x_n} f(x)\,dx = h\left\{\sum_{i=0}^{n} f_i - \frac{f_0+f_n}{2} - \frac{23681f_0 - 55688f_1 + 66109f_2 - 57024f_3 + 31523f_4 - 9976f_5 + 1375f_6}{120960} - \frac{23681f_n - 55688f_{n-1} + 66109f_{n-2} - 57024f_{n-3} + 31523f_{n-4} - 9976f_{n-5} + 1375f_{n-6}}{120960}\right\} \tag{13}$$

This is an eight-order accurate integration scheme, exact for a seventh order polynomial. (The author would like to thank Dr. Michael D. White of the Ohio Aerospace Institute for providing this formula.) The calculations were marched in time until the change of the ionization frequency and the independent variables with each time step had reached a minimum.

The computational domain was taken to be $L = 100\lambda_D$ in width, and a reference computation was carried out with a grid of 401 points using the E4-AC4-C6-AC4-E4 compact difference scheme. Figure 4a shows the ion and electron number densities and the ion temperature. The quasi-neutral presheath (where $n_i \approx n_e$) is apparent near the centerline, and the sheath (where $n_e \approx 0$) is visible near the electrode on the left. The ion temperature rises near the electrode due to the dissipative effects of elastic ion-neutral collisions (see Eq. 4a).

The electric potential and ion velocity are shown in Fig. 4b. The majority of the potential drop occurs in the sheath, with only a slight change in the presheath. Despite the collisional drag with the neutrals, the ions are seen to be strongly accelerated toward the electrode by the electric field in the sheath.

The error in the ionization rate z, relative to the reference solution, was chosen as a figure of merit for spatial convergence. The results of the convergence study are shown in Fig. 4c. The convergence behavior of the two schemes is seen to be similar to that observed in the previous examples.

D. Shock Structure with Three-Species Model

As a final test, a computation involving a three-species model of a shock in a weakly-ionized, nonequilibrium plasma was carried out. The flow conditions were chosen to be similar to those examined by Adamovich et al.[32] The upstream conditions for the neutrals were $u_1 = 645$ m/s, $p_1 = 1.3$ kPa, and $T_1 = 300$ K. The electron temperature was taken to be $T_e = 3.6$ eV, and the fractional ionization in the incoming flow was $n_{i,e}/n_n = 1 \times 10^{-6}$. The electric potential was set to zero at the upstream boundary, and extrapolation was used for all quantities at the downstream boundary. Ideal gas jump relations were used for the initial conditions.

As with the previous problems, the electrons were assumed to be in Boltzmann equilibrium. Ionization and recombination rates were chosen to match those of Adamovich et al.

The computational domain was $L = 5$ mm wide, and a grid of 1001 points was employed. The E4-AC4-C6-AC4-E4 compact difference scheme was used. For stability, Filter B was employed, and second-order extrapolation was used for the outlet boundary condition.

The results of the computations are shown in Fig. 5. Figure 5a shows the number density for each species and the electric potential. The velocity for each species is shown in Fig. 5b, and the corresponding temperatures in Fig. 5c. The shock transition zone is seen to be substantially thicker for the charged particles than for the neutral gas. The large difference in mass between the ions and electrons leads to charge separation in the vicinity of the neutral gas jump, setting up an electric potential rise of a few volts across the shock.

IV. Summary and Conclusions

This paper has explored the feasibility of applying high-order, compact difference methods to the modeling of glow discharges for high-speed flow control. High-order compact difference methods offer a possible means of achieving high spatial accuracy on coarser grids, potentially leading to a significant reduction in the computational cost of an accurate solution. Sample calculations were presented for shock and sheath problems in ionized argon, and the compact difference methods were shown to be superior in both absolute accuracy and rate of spatial convergence. Future work will focus on applying the compact difference method to problems of interest in plasma aerodynamics.

Acknowledgments

This project is sponsored in part by the Air Force Office of Scientific Research (monitored by F. Fahroo), and by a grant of High Performance Computing time from the Air Force Research Laboratory Major Shared Resource Center. The author would like to acknowledge helpful discussions of this ongoing project with D. Gaitonde and M. White.

References

[1]Surzhikov, S. T. and Shang, J. S., "Two-Component Plasma Model for Two-Dimensional Glow Discharge in Magnetic Field," *Journal of Computational Physics*, Vol. 199, 2004, pp. 437–464.

[2]Mahadevan, S. and Raja, L. L., "Simulations of Glow Discharge Phenomena in Air for High-Speed Flow Control," AIAA Paper 2008-1093, American Institute of Aeronautics and Astronautics, Reston VA, January 2008.

[3]Poggie, J., "Numerical Simulation of Direct Current Glow Discharges for High-Speed Flow Control," *Journal of Propulsion and Power*, Vol. 24, No. 5, 2008, pp. 916–922.

[4]Poggie, J., "Numerical Simulation of DC and RF Glow Discharges," AIAA Paper 2007-0632, American Institute of Aeronautics and Astronautics, Reston VA, January 2007.

[5]Poggie, J., "Discharge Modeling for Flow Control Applications," AIAA Paper 2008-1357, American Institute of Aeronautics and Astronautics, Reston VA, January 2008.

[6]Lele, S. K., "Compact Finite Difference Schemes with Spectral-Like Resolution," *Journal of Computational Physics*, Vol. 103, 1992, pp. 16–42.

[7]Gaitonde, D. V. and Visbal, M. R., "High-Order Schemes for Navier-Stokes Equations: Algorithm and Implementation in FDL3D," AFRL Technical Report AFRL-VA-WP-TR-1998-3060, Air Force Research Laboratory, Wright-Patterson Air Force Base, Ohio, 1998.

[8]Ward, A. L., "Calculations of Cathode-Fall Characteristics," *Journal of Applied Physics*, Vol. 33, No. 9, 1962, pp. 2789–2794.

[9]Ward, A. L., "Effect of Space Charge in Cold-Cathode Gas Discharges," *Physical Review*, Vol. 112, No. 6, 1958, pp. 1852–1857.

[10]Boeuf, J.-P., "A Two-Dimensional Model of DC Glow Discharges," *Journal of Applied Physics*, Vol. 63, No. 5, 1988, pp. 1342–1349.

[11]Raizer, Y. P. and Surzhikov, S. T., "Two-Dimensional Structure in a Normal Glow Discharge and Diffusion Effects in Cathode and Anode Spot Formation," *High Temperature*, Vol. 26, No. 3, 1988, pp. 304–311.

[12]Passchier, J. D. P. and Goedheer, W. J., "A Two-Dimensional Fluid Model for an Argon RF Discharge," *Journal of Applied Physics*, Vol. 74, No. 6, 1993, pp. 3744–3751.

[13]Young, F. F., "Two-Dimensional, Self-Consistent, Three-Moment Simulation of RF Glow Discharges," *IEEE Transactions on Plasma Science*, Vol. 21, No. 3, 1993, pp. 312–321.

[14]Hong, M. and Emmert, G. A., "Two-Dimensional Fluid Modeling of Time-Dependent Plasma Sheath," *Journal of Vacuum Science and Technology*, Vol. 12, No. 2, 1994, pp. 889–896.

[15]Sheridan, T. E. and Alport, M. J., "Two-Dimensional Model of Ion Dynamics During Plasma Source Ion Implantation," *Applied Physics Letters*, Vol. 64, No. 14, 1994, pp. 1783–1785.

[16]Georghiou, G. E., Papadakis, A. P., Morrow, R., and Metaxas, A. C., "Numerical Modelling of Atmospheric Pressure Gas Discharges Leading to Plasma Production," *Journal of Physics D: Applied Physics*, Vol. 38, 2005, pp. R303–R328.

[17]Graves, D. B. and Jensen, K. F., "A Continuum Model of DC and RF Discharges," *IEEE Transactions on Plasma Science*, Vol. PS-14, No. 2, 1986, pp. 78–91.

[18]Richards, A. D., Thompson, B. E., and Sawin, H. H., "Continuum Modeling of Argon Radio Frequency Glow Discharges," *Applied Physics Letters*, Vol. 50, No. 9, 1987, pp. 492–494.

[19]Barnes, M. S., Cotler, T. J., and Elta, M. E., "A Staggered-Mesh Finite-Difference Numerical Method for Solving the Transport Equations in Low Pressure RF Glow Discharges," *Journal of Computational Physics*, Vol. 77, 1988, pp. 53–72.

[20]Hammond, E. P., Mahesh, K., and Moin, P., "A Numerical Method to Simulate Radio-Frequency Plasma Discharges," *Journal of Computational Physics*, Vol. 176, 2002, pp. 402–429.

[21]Meyyappan, M. and Kreskovsky, J. P., "Glow Discharge Simulation Through Solutions to the Moments of the Boltzmann Transport Equation," *Journal of Applied Physics*, Vol. 68, No. 4, 1990, pp. 1506–1512.

[22]Meyyappan, M., "A Continuum Model for Low-Pressure Radio-Frequency Discharges," *Journal of Applied Physics*, Vol. 69, No. 12, 1991, pp. 8047–8051.

[23]Widner, M., Alexeff, I., Jones, W. D., and Lonngren, K. E., "Ion Acoustic Wave Excitation and Ion Sheath Evolution," *The Physics of Fluids*, Vol. 13, No. 10, 1970, pp. 2532–2540.

[24]Sternberg, N. and Poggie, J., "Plasma-Sheath Transition in the Magnetized Plasma-Wall Problem for Collisionless Ions," *IEEE Transactions on Plasma Science*, Vol. 32, No. 6, 2004, pp. 2217–2226.

[25]Poggie, J. and Sternberg, N., "Transition from the Constant Ion Mobility Regime to the Ion-Atom Charge-Exchange Regime for Bounded Collisional Plasmas," *Physics of Plasmas*, Vol. 12, No. 2, 2005, pp. 023502–1–023502–9.

[26]Burgers, J. M., *Flow Equations for Composite Gases*, Academic Press, New York, 1969.

[27]Appleton, J. P. and Bray, K. N. C., "The Conservation Equations for a Non-Equilibrium Plasma," *Journal of Fluid Mechanics*, Vol. 20, No. 4, 1964, pp. 659–672.

[28]Chapman, S. and Cowling, T. G., *The Mathematical Theory of Non-Uniform Gases*, Cambridge University Press, 2nd ed., 1952.

[29]Morse, T. F., "Energy and Momentum Exchange between Nonequipartition Gases," *The Physics of Fluids*, Vol. 6, No. 10, 1963, pp. 1420–1427.

[30]Yuan, X. and Raja, L. L., "Computational Study of Capacitively Coupled High-Pressure Glow Discharges in Helium," *IEEE Transactions on Plasma Science*, Vol. 31, No. 4, 2003, pp. 495–503.

[31]Lister, G. G., "Low-Pressure Gas Discharge Modelling," *Journal of Physics D*, Vol. 25, No. 12, 1992, pp. 1649–1680.

[32]Adamovich, I. V., Subramaniam, V. V., Rich, J. W., and Macheret, S. O., "Phenomenological Analysis of Shock-Wave Propagation in Weakly Ionized Plasmas," *AIAA Journal*, Vol. 36, No. 5, 1998, pp. 816–822.

[33]White, F. M., *Viscous Fluid Flow*, McGraw-Hill, New York, 2nd ed., 1991.

[34]Hoffmann, K. A. and Chiang, S. T., *Computational Fluid Dynamics*, Engineering Educational System, Wichita KS, 4th ed., 2000.

[35]Anderson, W. K., Thomas, J. L., and van Leer, B., "A Comparison of Finite Volume Flux Vector Splittings for the Euler Equations," AIAA Paper 85-0122, American Institute of Aeronautics and Astronautics, Reston VA, January 1985.

[36]Cheney, W. and Kincaid, D., *Numerical Mathematics and Computing*, Brooks/Cole Publishing, Pacific Grove, California, 3rd ed., 1994.

[37]White, F. M., *Fluid Mechanics*, McGraw-Hill, New York, 1986.

[38]Zel'dovich, Y. B. and Raizer, Y. P., *Physics of Shock Waves and High-Temperature Hydrodynamic Phenomena*, Dover, Mineola NY, 2002, Reprint of 1967 translation, with corrections.

[39]Thompson, P. A., *Compressible-Fluid Dynamics*, McGraw-Hill, New York, 1972, Reprinted by author, 1988.

[40]Poggie, J. and Gaitonde, D. V., "Electrode Boundary Conditions in Magnetogasdynamic Flow Control," AIAA Paper 2002-0199, American Institute of Aeronautics and Astronautics, Reston VA, January 2002.

[41]Poggie, J., Gaitonde, D. V., and Sternberg, N., "Numerical Simulation of Plasma Sheaths in Aerodynamic Applications," AIAA Paper 2002-2166, American Institute of Aeronautics and Astronautics, Reston VA, May 2002.

[42]Lieberman, M. A., "Model of Plasma Immersion Ion Implantation," *Journal of Applied Physics*, Vol. 66, No. 7, 1989, pp. 2926–2929.

Scheme	α	a	b	Stencil	Order
E2	0	1	0	3	2
E4	0	4/3	-1/3	5	4
C4	1/4	3/2	0	3	4
C6	1/3	14/9	1/9	5	6

Table 1. Coefficients for compact difference schemes at interior points. Adapted from Gaitonde and Visbal.[7]

Scheme	Filter A	Filter B
E2-DE2-E2-DE2-E2	F0-$FB_{2,4}$-F4-$FB_{2,4}$-F0	F0-F2-F4-F2-F0
E4-DE4-E4-DE4-E4	F0-$FB_{2,6}$-$FB_{3,6}$-F6-$FB_{3,6}$-$FB_{2,6}$-F0	F0-F2-F4-F6-F4-F2-F0
E4-AC4-C4-AC4-E4	F0-$FB_{2,6}$-$FB_{3,6}$-F6-$FB_{3,6}$-$FB_{2,6}$-F0	F0-F2-F4-F6-F4-F2-F0
E4-AC4-C6-AC4-E4	F0-$FB_{2,6}$-$FB_{3,8}$-$FB_{4,8}$-F8-$FB_{4,8}$-$FB_{3,8}$-$FB_{2,6}$-F0	F0-F2-F4-F6-F8-F6-F4-F2-F0
E6-AC6-C6-AC6-E6	–	–

Table 2. Compact difference schemes and corresponding filters. Notation of Gaitonde and Visbal.[7]

Scheme	a_0	a_1	a_2	$a3$	a_4	Order
F2	$\frac{1+2\alpha_f}{2}$	$\frac{1+2\alpha_f}{2}$	0	0	0	2
F4	$\frac{5+6\alpha_f}{8}$	$\frac{1+2\alpha_f}{2}$	$\frac{-1+2\alpha_f}{8}$	0	0	4
F6	$\frac{11+10\alpha_f}{16}$	$\frac{15+34\alpha_f}{32}$	$\frac{-3+6\alpha_f}{16}$	$\frac{1-2\alpha_f}{32}$	0	6
F8	$\frac{93+70\alpha_f}{128}$	$\frac{7+18\alpha_f}{16}$	$\frac{-7+14\alpha_f}{32}$	$\frac{1-2\alpha_f}{16}$	$\frac{-1+2\alpha_f}{128}$	8

Table 3. Coefficients for filter schemes at interior points. Adapted from Gaitonde and Visbal.[7]

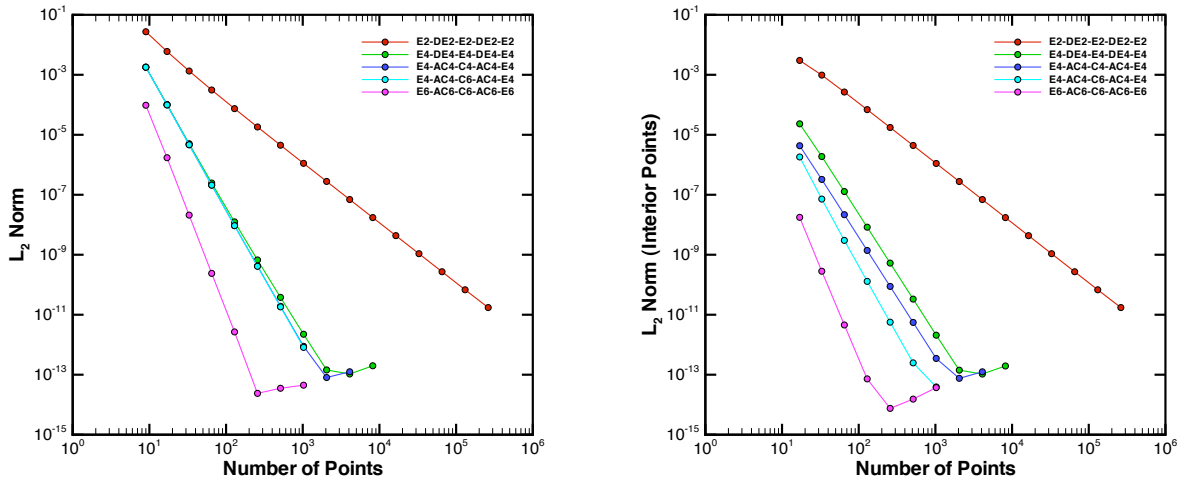

(a) L_2-norm for full domain.

(b) L_2-norm for interior points only.

Figure 1. Accuracy of $(\sin x)'$ with various compact difference schemes (see Table 2).

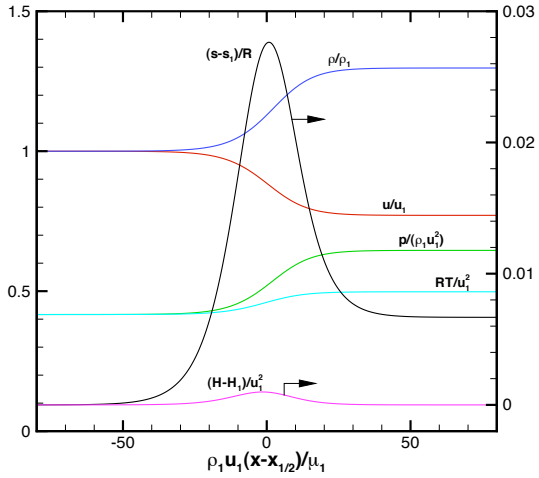

(a) Basic shock structure, computed with E4-AC4-C6-AC4-E4 scheme.

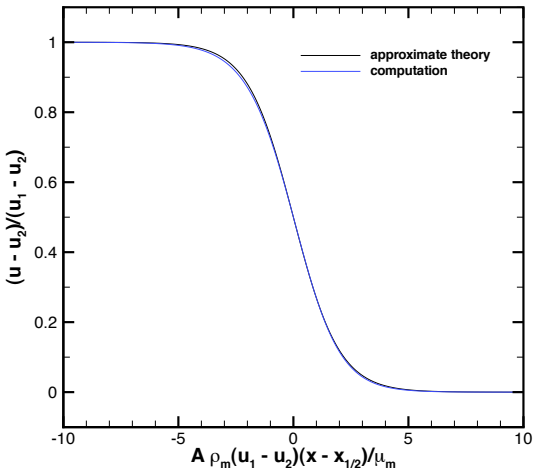

(b) Comparison of approximate theory to computation with E4-AC4-C6-AC4-E4 scheme.

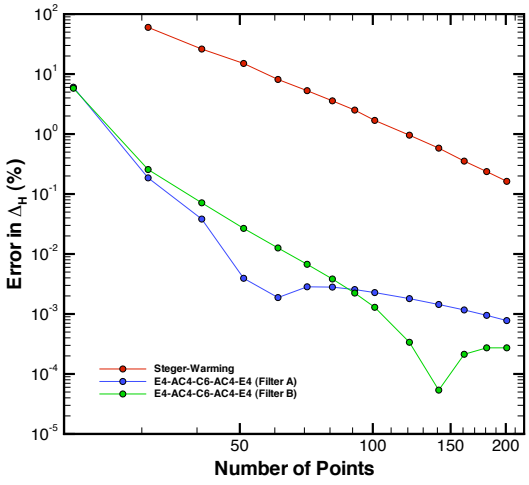

(c) Spatial convergence for two numerical schemes.

Figure 2. Shock structure in argon at Mach 1.2.

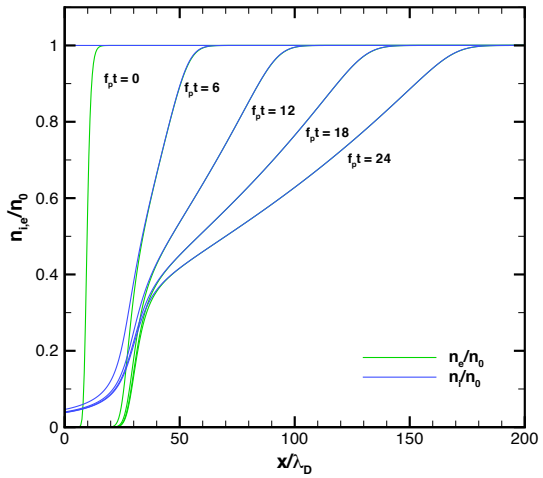

(a) Ion and electron number densities at selected times, E4-AC4-C6-AC4-E4 scheme.

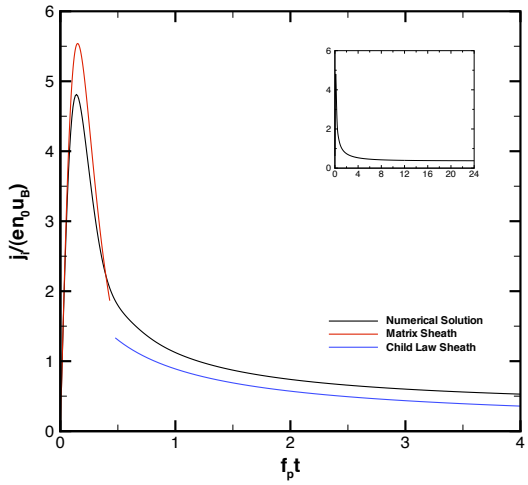

(b) Time-history of ion current at negative electrode, numerical results with E4-AC4-C6-AC4-E4 scheme.

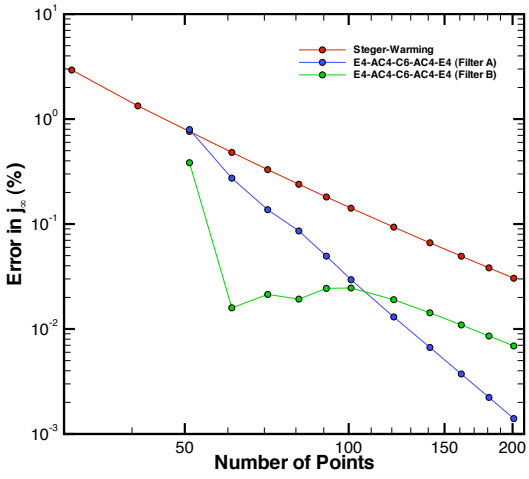

(c) Convergence of asymptotic ion current at electrode, $j(x = 0, t = 24)$.

Figure 3. Evolution of transient sheath.

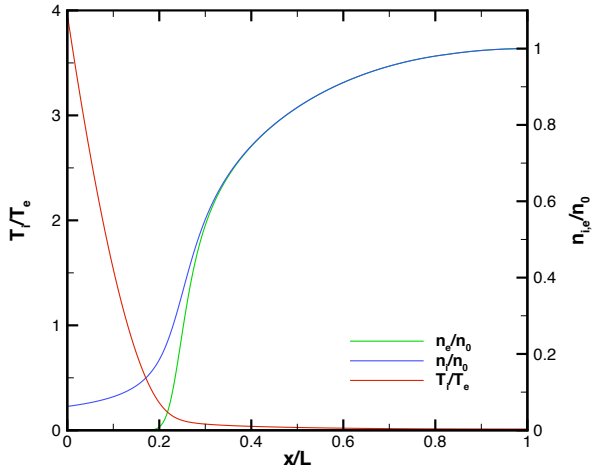

(a) Ion and electron number densities, ion temperature.

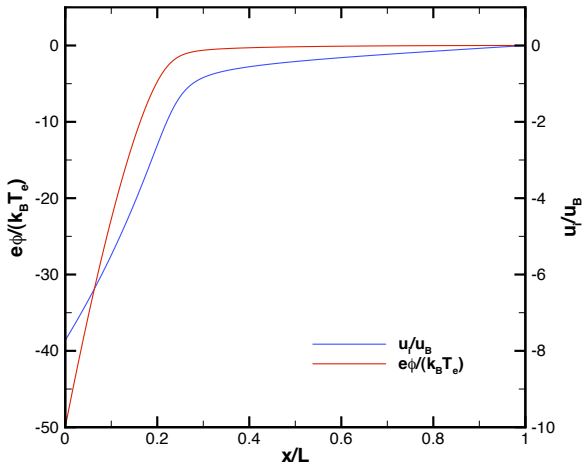

(b) Electric potential and ion velocity.

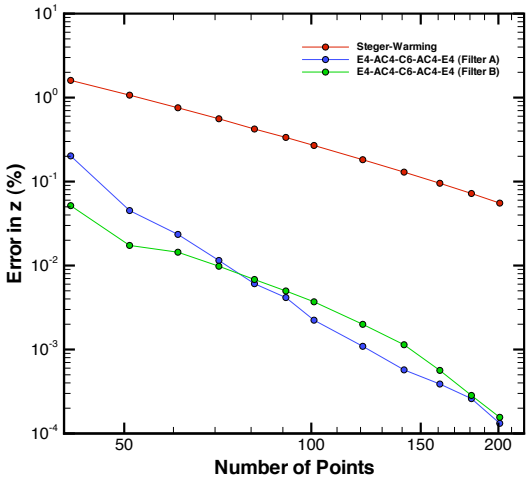

(c) Convergence of ionization rate.

Figure 4. Steady-state plasma-sheath problem.

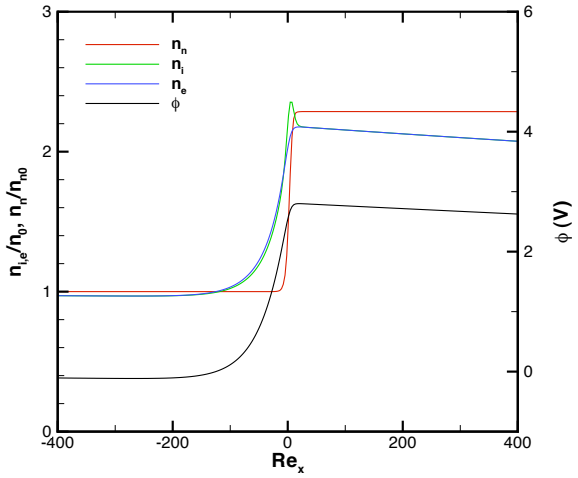

(a) Number densities and electric potential.

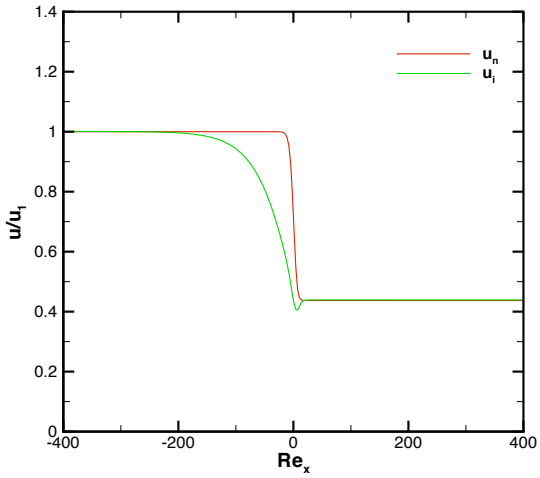

(b) Velocity.

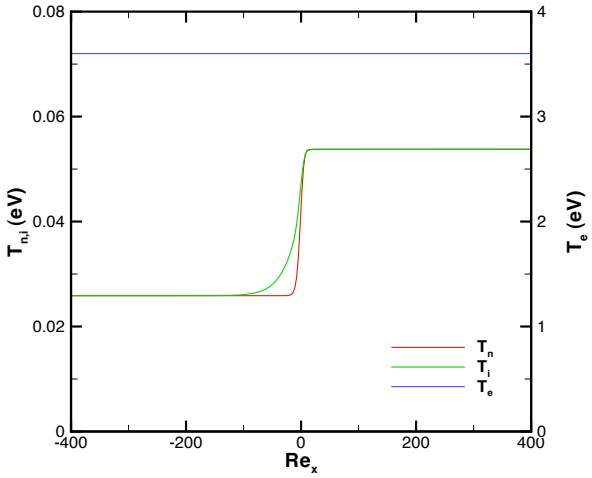

(c) Temperature.

Figure 5. Three-species model of shock structure.